Role of calcium-phosphate deposition in vascular smooth muscle cell calcification.

Ricardo Villa-Bellosta[1], Ángel Millán[2], Víctor Sorribas[1]*

[1]Laboratory of Molecular Toxicology, University of Zaragoza, Zaragoza, Spain. [2]ICMA, CSIC-University of Zaragoza, Zaragoza, Spain.

Running title: Calcium phosphate deposition in vascular cells

*Corresponding author: Laboratory of Molecular Toxicology, University of Zaragoza. Calle Miguel Servet 177, 50013 Zaragoza, Spain. Telephone (34) 976761631; Fax (34) 976761612; e-mail: sorribas@unizar.es

ABSTRACT

In this work we are studying if calcium phosphate deposition (CPD) during vascular calcification is a passive or a cell-mediated mechanism. Passive CPD was studied in fixed vascular smooth muscle cells (VSMC), which calcify faster than live cells in the presence of 1.8 mM Ca^2+ and 2 mM Pi. CPD seems to be a cell-independent process that depends on the concentration of calcium, phosphate, and hydroxyl ions, but not on Ca x Pi concentration products, given that deposition is obtained with 2x2 and 4x1 Ca x Pi mM^2 but not with 2x1 or 1x4 Ca x Pi mM^2. Incubation with 4 mM Pi without CPD (i.e., plus 1 mM Ca) does not induce osteogene expression. Increased expression of bone markers such as Bmp2 and Cbfa1 is only observed concomitantly with CPD. Hydroxyapatite is the only crystalline phase in both lysed and live cells. Lysed cell deposits are highly crystalline while live cell deposits still contain large amounts of amorphous calcium. High-resolution transmission electron microscopy revealed a nanostructure of rounded crystallites of 5-10 nm oriented at random in lysed cells, which is compatible with spontaneous precipitation. The nanostructure in live cells consisted of long fiber crystals, 10-nm thick, embedded in an amorphous matrix. This structure indicates an active role of cells in the process of hydroxyapatite crystallization. In conclusion, our data suggest that CPD is a passive phenomenon, which triggers the osteogenic changes that are involved in the formation of a well organized, calcified crystalline structure.

Keywords

Vascular calcification; hyperphosphatemia; crystal structure; calcium phosphate deposition; vascular smooth muscle cell.

INTRODUCTION

Considerable efforts have been made over the last decade to understand the pathogenesis of vascular calcification (VC). It is now generally accepted that medial mineralization of the arteries (i.e., Mönckeberg's sclerosis) is an orchestrated phenomenon that resembles the ossification processes of the bone (4, 30). The phenomenon includes the transdifferentiation of vascular smooth muscle cells (VSMC) to a phenotype with osteogenic characteristics as a response to uremic toxins and hyperphosphatemia in chronic kidney disease (CKD) or in diabetes (9, 17).

Despite the significant amount of knowledge in the field, important questions remain to be answered. For example, one of the key questions that is still unclear refers to whether calcification is an actively promoted phenomenon or an actively inhibited phenomenon (27, 28). Regarding the former possibility, physiological (e.g., bone) and ectopic calcifications take place after the expression of a mineralizing extracellular matrix (ECM) and after stimulation by hormonal and non-hormonal factors (28). Calcification is therefore an active process. Regarding the latter possibility, calcification could occur as a consequence of the absence (bone) or loss (VC) of calcification inhibitors, and therefore calcium phosphate deposition occurs as a passive phenomenon (28). In this case, mineralization is actively inhibited and prevented in the arteries under physiological conditions. A key finding that supports the loss-of-inhibition hypothesis of VC is the observation that a knock-out mouse carrying the VC inhibitor, matrix-Gla protein, shows extensive calcification of soft tissues, even in the presence of normal blood concentrations of Ca^{2+} and Pi (15). This hypothesis is further supported by the fact that the concentrations of Ca^{2+} and Pi exceed the solubility product in the extracellular milieu (19), and therefore in the presence of such metastable fluids, mineralization should start as soon as local calcification inhibitors are eliminated (20). However, the problem of ectopic calcification can apparently not be explained exclusively by either possibility, given that the expression of both mineralization activators during VC and the expression of inhibitors under physiological circumstances have been demonstrated.

One of the key players in the pathogenesis of VC in CKD is Pi, but its specific pathogenic role is still unclear despite extensive work over the last decade. In this paper we have done an *in vitro* study of the pathogenesis of Pi-induced calcification by analyzing the extent of cellular activity involvement during

initial calcium phosphate deposition (CPD) and by studying the relative role of the osteogenic changes in the process. We have concluded that while CPD is a passive phenomenon that depends on the absence of calcification inhibitors, CPD is also responsible for the osteogenic changes that build a biomineralized deposit with a crystalline nanostructure that is very different from the crystalline nanostructure of passive mineralization.

MATERIALS AND METHODS

Cell culture

The isolation and culture conditions of rat aorta VSMC, as well as opossum kidney cells (OK), have been described previously (37, 38). The protocols were submitted to and approved by the Ethics Committee of the University of Zaragoza. Cells were grown to confluence and used after an overnight quiescence step. For calcification, cells were plated in 24-well dishes. VSMC were grown in a minimum essential medium (MEM), and OK cells were grown in DMEM/F12. Both MEM and DMEM/F:12 were supplemented with glutamine and 10% fetal calf serum. All cell culture reagents were from Invitrogen (Paisley, UK). For the preparation of customized (synthetic) MEM (sMEM), the inorganic salt, D-glucose (Dextrose), amino acid, and vitamin components of the MEM culture medium were obtained separately from Invitrogen. The final concentrations correspond to the composition of the MEM: 0.814 mM of magnesium sulfate ($MgSO_4$), 5.33 mM of potassium chloride (KCl), 26.19 mM of sodium bicarbonate ($NaHCO_3$), 117.24 mM of sodium chloride (NaCl), and 1000 mg/L of D-glucose.

Calcification determination

Calcification of VSMC was performed as described, including the preparation and use of lysed cells (39), except for 24-hour preincubation with 2 mM Pi before lysis, which we found to be unnecessary (see Results). Both live and fixed cells were calcified in an identical way, and the same calcification medium was used, which contained 0.5% FCS. In this work, identical results were obtained by paraformaldehyde fixation and overnight drying. As a negative control, a plate without cells was always used in the experiments. The calcification of VSMC was identified by Alizarin red staining and was quantified using a QuantiChrom^{TM} Calcium Assay Kit (BioAssay Systems, Hayward, CA).

Collagen and elastin calcification

A rat type I collagen solution was obtained from Invitrogen, and a soluble human elastin, fraction V bovine albumin, and poly-L-lysine were obtained from Sigma-Aldrich. The collagen, elastin, and albumin were fixed to a plastic cell culture support at 5 μg/cm^2 following the collagen manufacturer's instructions

(Invitrogen). The poly-L-lysine coating was applied following the classical protocol for cell culture. Calcification was then performed as it was for the cells.

Real time PCR

The relative quantification of Msx2, Cbfa1, Bmp2, and SM22 alpha was performed by real-time PCR using SYBR Green on a LightCycler (Roche Applied Science, Mannheim, Germany), following the manufacturer's instructions for calibrator normalized protocols as described (40). The primers used to amplify Msx2, Cbfa1, and Bmp2 have been listed previously (41). SM22α was amplified using CAGACTGTTGACCTCTTTGAAG as the upper primer and TCTTATGCTCCTGGGCTTTC as the lower primer. The acidic ribosomal phosphoprotein (Arp) RNA was used as an endogenous reference (40).

Analysis of calcification composition

The composition, microstructure, and crystal structure of the deposits were characterized by X-ray powder diffraction (XRD; Rigaku D-max B), scanning electron microscopy (SEM; JEOL 6400) equipped with an INCA-300 energy dispersive spectroscopy (EDS) system (Oxford Instruments), transmission electron microscopy (JEOL 2000FXII) equipped with an INCA-200 microanalysis system (Oxford Instruments), and high-resolution electron microscopy (FEI TECNAI G2 F30). Samples for XRD were prepared by spreading ground powders on a glass holder. Samples for the structural characterization were prepared by collecting deposits from 6-well plates for each live and lysed cell cultures and then mixing them in a mortar. XRD analysis was performed on ground powders spread on a glass holder. For TEM analysis, powders were dispersed in hexane, and the dispersion was evaporated on a carbon-coated microscope grid. Samples for SEM observations were prepared by gluing pieces of the culture recipient bottom and coating them with gold or carbon. Part of the samples was washed repeatedly with water by decantation to eliminate any soluble substance present in the sample before observation.

Data analysis

The mean effective constants of calcification prevention were calculated by non-linear regression, thereby fitting data to a logarithmic dose-response curve (39). Each experiment was repeated at least three times with similar results. Data are shown as the mean ± SE. The significances of differences were evaluated by an analysis of variance and a Tukey's multicomparison post-test.

RESULTS

Passive versus active calcium phosphate deposition

We studied passive CPD (i.e., in the absence of any cellular activity or metabolism) using fixed VSMC (39). In this case, we did not preincubate the cells with 2 mM Pi for 24 hours before lysis, as initially described (39), because we found that dead cells calcified to the same extent, whether or not the cells were subjected to this previous treatment (data not shown). We compared the amount of CPD obtained using either live or fixed VSMC in the presence of a culture medium (MEM) containing 2 mM Pi (Fig. 1A). Calcium deposition increased significantly in fixed cells (black bars) after 3 days and significantly in live cells (open bars) after 5 days. At 3, 5, and 7 days, the amount of precipitated Ca^{2+} in fixed cells was three times the amount in live cells. This difference was then kinetically analyzed by comparing the dose-response effects of pyrophosphate on the prevention of calcification in both live and fixed cells (Fig. 1B). The Hill slopes of the curves were similar (-2.4 vs. -2.7 for live and fixed cells, respectively), but the ECs_{50} of PPi were very different: 2.6 and 8.8 μM for live and fixed cells, respectively. Therefore, more PPi is necessary to prevent calcification in fixed cells. Subtraction of both logarithmic curves provided a log normal distribution curve with a mean of 4.9 ± 1.0 μM and a standard deviation equivalent to the $Hill^{-1}$ slope (2.14). Several interpretations can explain the shift in EC_{50}, but it is most likely due to the amount of calcification inhibitors, such as PPi, which are produced by live cells and are missing in fixed cells. Similar findings were obtained in our previous work using bisphosphonates (39).

Next, we attempted to define the nature of the macromolecular matrix required for CPD and adsorption in the cells. VSMC were incubated in MEM with 2 mM Pi for up to 5 days (Fig. 2A), and every day a group of cells were trypsinized or lysed with the indicated detergents at 0.1%. The wells were then kept in the 2 mM Pi medium for the remaining days. The cells that were lysed with any of the three detergents calcified at the same intensity as from the first day of lysis. This suggests that calcification takes place predominantly in the protein phase of the cells, but a role by the lipid component cannot be excluded. Fig. 2B shows the calcium quantification after 7 days of incubation with 1 or 2 mM Pi, according to the indicated treatments.

Next, we directly studied the role of collagen and elastin, two extracellular proteins that are known to induce calcification. Rat collagen type I and human elastin were fixed onto cell culture plates and incubated with MEM containing either 1 or 2 mM Pi for seven days. Staining with Alizarin red revealed an intense calcification of all collagen fibers incubated with 2 mM Pi, as well as intense calcification of the globular elastin that was attached to the plastic surface, which concurs with previous *in vitro* and *in vivo* studies (Fig. 2C). Surface coating with albumin or poly-L-lysine did not induce CPD in the culture dishes. These results indicate that calcification can apparently be obtained with single molecules when specific experimental conditions are attained. However, as shown below, the definite crystal ultrastructure is only obtained when the active cell is present.

Role of the composition of the cell culture medium and of pH

In vitro calcification of VSMC is an established model of VC that, in some cases, has yielded significant differences in calcification rates among laboratories, as demonstrated by the use of different Pi concentrations (usually 2-4 mM Pi) in culture media to induce Pi-related VC. Therefore, before continuing with subsequent experiments, we checked to see if the composition of the different culture media could be at least partially responsible for these differences. We obtained identical qualitative results using either live or lysed cells. VSMC were induced to calcify using 2 mM Pi by supplementing the phosphate concentration of three different culture media: MEM, DMEM, and DMEM/F:12. Figure 3A shows that the calcification induced using 2 mM Pi (black bars) was only obtained with MEM or DMEM, while cells incubated with DMEM/F:12 did not calcify. Comparison of the media revealed that MEM and DMEM contain 1.8 mM Ca^{2+}, while DMEM/F:12 contains only 1.05 mM. DMEM/F:12 was subsequently supplemented to reach a final concentration of 1.8 mM Ca^{2+}, after which calcification was successfully induced using 2 mM Pi (Fig. 3B) at pH 7.5 or higher (pH 8.0). In this study we only used fixed VSMC to maintain a constant pH. No calcification was observed at pH 7.0 or in cells incubated using 1 mM Pi at any of the three pHs. Therefore, while VSMC cultures can be a valuable model for studying cell-mediated calcification, it is essential to observe standardized experimental conditions and the use of similar culture media. In any event, this finding does not invalidate the knowledge obtained with these cultures during the last decade.

While the effect of pH on calcification has been extensively studied, we nevertheless performed an additional experiment to understand the pathogenesis of CPD. Opossum Kidney (OK) cells constitute a proximal tubular cell line that is known to quickly acidify culture medium, even below pH 7.0. Consequently, when OK cells were incubated with DMEM/F:12 (the usual culture medium) containing 1.8 mM Ca^{2+} and 2 mM Pi, they did not calcify (Figure 3C). In contrast, when we used fixed OK cells, the pH did not change and calcification occurred at a rate similar to the VSMC rate. While there are other possibilities in addition to pH, such as the presence of calcification inhibitors, this finding suggests that the expression of a specific extracellular matrix is not necessary to initiate CPD and that calcification will take place in any cell in the absence of anticalcifying agents such as pyrophosphate or an acidic milieu.

Effects of pH and Ca x Pi products on in vitro calcification

Apart from pH, the Ca x Pi concentration product is another parameter that affects calcification, and while it is generally considered to be a risk factor in hemodialysis patients, there is also growing controversy about its significance (19). We studied the validity of this parameter using the passive CPD model, because fixed VSMC allow the use of a supraphysiological concentration of Ca^{2+} and Pi. VSMC were incubated for six days in a DMEM/F:12 medium supplemented with different concentrations of Ca^{2+} and Pi (1, 2, or 4 mM, Fig. 3D). No calcification was observed when the Ca x Pi molar product was kept below 4 mM, in any combination. Calcification was observed when a 4 mM Ca x Pi product was obtained by combining 2 mM Ca^{2+} and 2 mM Pi, or 4 mM Ca^{2+} and 1 mM Pi. No calcification was observed when the 4 mM Ca x Pi product was obtained with 1 mM Ca^{2+} and 4 mM Pi.

These results point to a predominant role of Ca^{2+} over Pi during calcification, as it has been reported previously (42) and very recently while our work was under review (33). A more detailed analysis of the calcium effect was studied on fixed VSMC so that non-physiological concentrations of Ca and Pi could be used. VSMC were incubated in the presence of a constant concentration of 1 mM Pi, with increasing concentrations of Ca^{2+} (Fig. 4A). Under these conditions, no saturation was obtained, but calcification increased with the increasing Ca^{2+} concentration. Conversely, when the concentration of Ca^{2+} was fixed at 1.5, 1.8, or 2.0 mM, the calcification obtained by increasing the concentration of Pi was saturated (maximal) at 3 mM Pi and 2 mM Ca^{2+} (Fig. 4B). The predominance of Ca^{2+} over Pi can be explained in

physiochemical terms (see Discussion), considering that the cells were lysed and therefore any effect by calcium signaling can be discarded.

Calcifying components of the culture medium

Based on the varying extent of the calcification obtained using the different basal culture media and the dependence of calcification on the calcium content, we attempted to determine the involvement of the other components of the culture media in *in vitro* calcification. We once again used lysed VSMC so that non-physiological conditions could be used in the experiments. Cells were incubated in MEM or in the different components of this basal medium, supplemented (or not) with phosphate to finally obtain 2 mM Pi. When the following components were combined, a synthetic MEM (sMEM) was obtained, as explained in Methods: a salt component (SC) and SC plus amino acids, vitamins, or glucose (Fig. 4C). In the presence of 2 mM Pi, calcifications were observed in all combinations, and the addition of amino acids and vitamins did not alter the extent of calcification. The involvement of the MEM salt component in calcification was further analyzed by combining the various components and by incubating fixed VSMC for six days using 1.8 mM Ca^{2+} plus 2 mM Pi (Fig. 4D). NaCl, KCl, and $MgSO_4$, either individually or combined, reduced the deposition of calcium induced with Ca and Pi. Conversely, the bicarbonate ion increased calcium deposition as expected, independently of any other ion present in the medium. The pH of the medium was kept at a constant 7.4 using 10 mM Hepes-Tris, and it was checked using a pH-meter. In summary, choosing the correct culture medium is a critical factor when performing *in vitro* calcification assays.

Calcium phosphate deposition induces osteogenic changes

The preceding findings on CPD and Ca x Pi products led us to compare the effects of different conditions on osteogene expression and on the transdifferentiation of VSMC during calcification. Specifically, we could now study the effects of CPD on osteogene expression separately from the effects of a high Pi concentration on osteogene expression. VSMC were incubated for 24 hours with MEM containing 1.8 mM Ca^{2+}, plus either 1 or 2 mM Pi, and then the abundance of Bmp2, Cbfa1, Msx2, and Osx was determined by using real-time PCR. Fig. 5A shows that, after just one day of incubation, the expression of Cbfa1,

Msx2, and Osx was significantly increased. The abundance increased thereafter (including Bmp2), and it was very strong after 5 days (Fig. 5B), when calcification was very intense (see Fig. 1A).

For a more detailed analysis of the effects of Ca x P, different combinations of Ca^{2+} and Pi were used to study the osteogene expression response in VSMC (Fig. 5C). VSMC were incubated for three days in sMEM in the presence of either 2 mM Ca^{2+} plus 1 mM Pi, 2 mM Ca^{2+} plus 2 mM Pi, 1 mM Ca^{2+} plus 4 mM Pi, or 4 mM Ca^{2+} plus 1 mM Pi. The combinations that induced calcification (2 mM Ca^{2+} plus 2 mM Pi and 4 mM Ca^{2+} plus 1 mM Pi) were the only ones to increase the abundance of Bmp2 and Cbfa1, while the expression of the smooth muscle marker SM22α decreased. When the concentration of Pi was increased to 4 mM and the concentration of Ca^{2+} was decreased to 1 mM to avoid calcification (see Fig. 3D), no significant changes in the abundances of Cbfa1, Bmp2, or SM22α were observed compared to the control (2 mM Ca^{2+} plus 1 mM Pi). These findings demonstrate that the increased extracellular concentration of Pi is not responsible for changes in osteogene expression in VSMC, but rather the initial deposition of calcium phosphates is responsible for the changes.

Analysis of calcium phosphate deposits

The calcifications obtained in live and lysed cells were analyzed to check whether the final composition of the mineralization process (i.e., after CPD) was similar in both situations. Significant differences between the compositions in both experimental situations would indicate the active involvement of transdifferentiated cells in the process. The crystal structure of deposits of live and fixed cells were analyzed by x-ray powder diffraction. XRD patterns from live and fixed samples showed narrow peaks corresponding to a halite structure (NaCl). Patterns of samples after washing are shown in Fig. 6A. The broad band centered at 22^{o} arises from the glass holder. The rest of the peaks correspond to nanometric crystals, and they can be indexed according to an apatite crystal structure, in both live and lysed VSMC.

The composition and microstructure of the deposits in live and lysed VSMC were analyzed by SEM (Fig. 6B and C). The surface of the deposits was flat, especially in living cell cultures, and it was formed by compact arrangements of spherolite-shaped particles.

EDS analyses showed the presence of P, Ca, Mg, Cl, and Na in both live and lysed cell samples. However, the Ca/P atomic ratios were different in lysed and live cell deposits. In lysed cells the Ca/P ratio

was close to 1.7 (mean = 1.72, SD = 0.16), which is the ratio corresponding to the hydroxyapatite compound ($Ca_{10}(PO_4)_6(OH)_2$) and which explains the presence of the Mg that is often found in this compound. In live cells this ratio significantly decreased (mean = 1.40, SD = 0.21), whereas the O/P ratio increased, indicating the presence of calcium-deficient compounds with a high degree of hydration [such as amorphous calcium phosphate ($Ca_9(PO_4)_6 \cdot nH_2O$; Ca/P = 1.5, O/P = 4.8), octacalcium phosphate ($Ca_8H_2(PO_4)_6 \cdot 5H_2O$; Ca/P = 1.33, O/P = 4.8), and dicalcium phosphate dihydrate or brushite ($CaHPO_4 \cdot 2H_2O$; Ca/P = 1.0, O/P = 6.0)] (16). The absence of these compounds in XRD patterns can be due to their amorphous character or to a small crystallite size.

Ultrastructural analysis of crystallites

A more detailed view of the microstructure was obtained by TEM and high-resolution TEM (HRTEM). Images at low resolution show planar formations in both types of deposits (Figs. 7A and 7C). However, high-resolution observations revealed that these formations are polycrystalline and that they have a very different degree of crystallization and crystallite shape in the deposits of live versus lysed cells. The insets of panels A and C are at higher magnifications and show granular and fibrillar structures, respectively. The nanostructure in lysed cell deposits consists of highly crystalline regions with a size of 5 to 10 nm and a rounded shape (Fig. 7B). However, live cells showed an amorphous or poorly crystalline background, which is crossed by long filaments that have well-defined crystal planes and a thickness of about 10 nm.

The orientation of the crystallites within the sheets was analyzed by direct measurement of the interplanar distances on atomic resolution HRTEM images and by Fast Fourier Transform (FFT) diffraction patterns from the images. Crystallites in lysed cell samples yielded 7 different d_{hkl} distances corresponding to the (300), (002), (112), (210), (211), (222), and (300) crystal planes of hydroxyapatite. All these planes were observed on FFT patterns (Fig 8A) that also showed 10 extra reflections that could be assigned to hydroxyapatite crystal structure. It is therefore apparent that hydroxyapatite is the only crystalline phase in the samples and that the crystallites are oriented at random with respect to the sheet plane. In live cell samples, the distances measured between planes parallel to the direction of elongation of the fiber-crystals were mainly close to 3.42 Å, which corresponds to d_{002} in hydroxyapatite (3.45 Å), although in some defected crystals the distance was slightly larger (up to 3.9 Å). Therefore, the direction of elongation of the fiber-crystals is perpendicular to [001]. This reflection was also present in all the FFT

285 patterns taken on both single-crystal and polycrystalline regions (Fig. 8B). FFT patterns showed an extra
286 reflection at 2.07 ± 0.04 Å, forming an angle of nearly 30^{o} with the (001) reflection that could be assigned
287 to d_{113} in hydroxyapatite (2.07 Å). Therefore, the crystals are oriented with their [-110] direction parallel to
288 the electron beam, and they are elongated along the [110] direction. Apart from the amorphous
289 background and the fiber-crystals, HRTEM images of lysed cell samples showed areas with bent parallel
290 grooves, as shown in Fig. 8C, that could be interpreted as intermediate stages of crystallization.

291

292

293

294

295

DISCUSSION

Medial vascular calcification is a degenerative disease that is highly prevalent among patients who are on hemodialysis or who have diabetes. Recently, many characteristics of ossified arteries have been described, including the activation of a transdifferentiation program of VSMC into cells with osteoblast-like properties and the expression of a calcifying ECM. Nevertheless, neither the pathogenic steps during VC nor the specific roles of some of the agents that are clearly involved (hyperphosphatemia, uremia, hyperglycemia, and aging) have yet to be fully understood (for reviews of these subjects see references 3, 5, 11, 14, 15, and 17).

For example, it is still unclear whether VC is an active degenerative process or, conversely, it is a passive phenomenon that the tissue attempts to control. In this work we have aimed to clarify this point by using lysed VSMC as a simple model of passive calcification. Our findings point to an intermediate possibility: CPD is a passive phenomenon that seems to take place when the abundance of calcification inhibitors are decreased, and this adsorption to the cells is a major step that initiates specific osteogene expression and trans-differentiation of VSMC into osteoblast-like cells. Such osteogenic changes seem to be responsible for the organized apatite crystal ultrastructure, which consists of an amorphous crystalline background crossed by long, fibrillar crystal planes.

Role of initial calcium phosphate deposition

Our conclusion that CPD is a passive phenomenon is based on several results. First, we have found that lysed VSMC calcify faster than live cells when they are incubated with 2 mM Pi in a MEM culture medium (Fig. 1). One new fact that we have unveiled is that it is not necessary to incubate live cells with 2 mM Pi for 24 hours before lysis so that they calcify after lysis (39). This finding means that the induction of calcifying genes and the formation of a specific ECM (i.e., calcification activators) are not requisites for the *initial* step in VC, i.e., calcium phosphate deposition. Under these *in vitro* conditions, it is necessary to add more PPi to lysed cells than to live cells in order to prevent Pi-induced calcification (Fig. 1B). This finding can be interpreted, but not exclusively, as the inability of lysed cells to produce calcification inhibitors (pyrophosphate, triphosphate, and other polyphosphates), wherefore additional PPi must be added during the assay to prevent calcification. As a whole, the finding that the induction of specific

calcification activators (i.e., specific osteogenes) is not necessary to initiate the calcification process, and that additional PPi is necessary in lysed cells to prevent calcification agrees with and supports the loss-of-inhibitors hypothesis of VC.

Additional results in this study also support the view that CPD is a passive phenomenon. CPD can simply start after combining a few components of the MEM cell culture medium. As shown in Fig. 4D, the calcium deposition obtained with 1.8 mM Ca^{2+} plus 2 mM Pi in water is decreased by the presence of Na^{+}, K^{+}, and Mg^{2+} ions in the assay, but it is increased with the addition of a bicarbonate ion. The Na^{+}, K^{+}, and Mg^{2+} ions can play a role in the onset of calcification, because several ion substitutions have been described regarding hydroxyapatite ($Ca_{10}(PO_4)_6(OH)_2$): Mg^{2+}, Sr^{2+}, Pb^{2+}, or Na^{+} for Ca^{2+}; carbonate or arsenate for phosphate; and F^{-} or Cl^{-} for OH^{-} (10). Therefore, in the calcification process each of these ions will determine the formation and final composition of calcium-phosphate deposits, and when calcification inhibitors or an acidic pH are neutralized, CPD will even start in non-VSMC (e.g., renal OK cells; Fig. 3C). Deposition depends on many other factors, but only minimally on the calcium-phosphate concentration product (19). In blood, while Ca and Pi concentrations exceed the solubility product for hydroxyapatite, these concentrations are not supersaturated, because blood composition is very complex: other ions and proteins are involved in solubility and deposition. In a quiescent *in vitro* model of VSMC, media composition is not as complex. Nevertheless, we have confirmed that this is also not a valid parameter *in vitro*, because the product of 4 mM^2 (Ca x P) is only critical when calcium is present at ≥ 2 mM and because a medium containing 1 mM Ca and 4 mM Pi does not result in calcium-phosphate deposition (Fig. 3D). This is based on calcium's predominant role over Pi (Fig. 4A and B) and on the relevance of hydroxyl ions (Fig. 4D) during calcium-phosphate deposition, which concurs with previous calcification studies (28) and with some works showing that hydroxyapatite is synthesized from brushite or octacalcium by adding calcium and hydroxyl ions (3, 16).

Another remarkable finding in this work is that the induction of osteogene expression and the transdifferentiation of VSMC *in vitro* are not caused by high Pi levels in culture media such as those observed during hyperphosphatemia, but rather they are caused by CPD. As shown in Fig. 3D, we have been able to increase the Pi concentration up to 4 mM without calcium phosphate deposition simply by reducing the calcium concentration to 1 mM. Under these conditions, no calcification was observed, the

expressions of Bmp2 and Cbfa1 were not induced, and there was no change in the abundance of the smooth muscle marker Sm22α (Fig. 5C). The expression of Bmp2 and Cbfa1 and the inhibition of Sm22α only occur concomitantly with CPD. This finding implies that not only does CPD precede changes in the osteogene expression characteristic of VC but also that deposition itself, rather than the concentrations of free Pi in the cell culture, is most likely responsible for the changes in gene expression and for the transdifferentiation of this *in vitro* model. These findings concur with previous studies that prevented Pi-induced osteogene expression using PFA (2, 11). The results had been interpreted as the inability of Pi to enter the cell and induce gene expression. However, considering that PFA is not an inhibitor of VSMC Pi transport but rather an inhibitor of CPD (39), those previous results (2, 11) can be now reinterpreted, because they suggest that osteogene expression is caused by calcium phosphate deposition. Our findings also agree with previous proposals of Prof. Shanahan, who suggested that calcium-induced microcalcifications in sites of apoptosis precedes the osteogenic differentiation of VSMC, and that this could be a universal initiation mechanism for both medial and intimal calcification (32).

Ultrastructural analysis of calcification crystals

While the initial steps in ectopic calcification (i.e., CPD) seem to constitute a passive phenomenon, an analysis of the calcification crystal structure has revealed that cells participate actively in the final outcome, because there are a series of important differences between the composition and structure of the calcification deposits in lysed and (metabolically active) live cells (Figs. 7-8). In both cases, however, apatite is the predominant phosphate crystalline compound, and at a micrometer level, deposits are composed of polycrystalline planar formations. Hydroxyapatite ($Ca_{10}(PO_4)_6(OH)_2$) is the most stable calcium phosphate phase, and it is the most frequent one in geological and biological mineralizations (5, 43). It precipitates directly only when the calcium phosphate ionic product is above the hydroxyapatite saturation point, but below the saturation point of intermediate CaP phases, such as octacalcium phosphate (OCP, $Ca_8H_2(PO_4)_6.5H_2O$). Otherwise, the hydroxyapatite formation process occurs after an initial precipitating phase of amorphous calcium phosphate, which has a low Ca/P ratio (1.5) and consists of $Ca_9(PO_4)_6$ clusters (Polner's cluster) arranged in low density fractal aggregates (31). These aggregates are gradually ordered into a crystalline hydroxyapatite structure with a Ca/P ratio of 1.68. This process can be very slow, especially in biological systems (5,43), but it can be accelerated by high Ca/P ratios

and a high pH. The theoretical equilibrium morphology of hydroxyapatite crystals consists of a {101} bipyramid with {100} prismatic lateral faces and {103} and {111} faces at the corners (6). However, the real morphology of crystals grown at nearly equilibrium conditions is that of hexagonal prisms bounded by {100} side faces, with elongation in the [001] direction (24, 35). Given that the solubility of hydroxyapatite in water is very low, crystal growth in aqueous solutions is usually far from equilibrium conditions. Consequently, critical supersaturation for nucleation is very high, the nucleation rate is also very high, and the crystal growth rate is very low. Thus, unless special methods are used, such as hydrothermal or slow diffusion, the morphology of hydroxyapatite crystals grown in aqueous media is far from the equilibrium morphology. Typical hydroxyapatite aqueous precipitates consist of spherulitic agglomerates of a) non-faceted needle crystals elongated along the [001] direction when the pH is abruptly increased (26) or b) (100) platy crystals for slow pH increase (12). Fast growth conditions favor a needle-like morphology (23), and crystallization from intermediate phases favor a planar morphology (43). Biomimetic hydroxyapatite precipitates also show spherulitic formations of platy crystals elongated along [001] (18). In physiological calcium phosphate biomineralizations (i.e., bones and teeth), the main phase is hydroxyapatite, although they may contain other intermediate phases (especially in bones). The main feature that distinguishes physiological crystallizations from pathological ones is that the particles are hierarchically ordered thanks to the templating effect of organic matrixes (14, 44). In pathological calcifications, hierarchical order is lost, although some texturing produced by the presence of an organic matrix is usually found. The same thing occurs in aortic calcifications, which show a stratified microstructure of concentric, inorganic layers bounded by an organic matrix (1, 8, 21, 29). The hydroxyapatite crystals are planar and are arranged in spherulitic formations. The crystallite size, around 2-10 nm, is much smaller than in physiological calcifications.

In our experiments of live vs. dead cell calcification, there are considerable differences in the crystal structure. CaP deposits from lysed cells show a hydroxyapatite atomic structure, a slight presence of amorphous calcium phosphate, a high Ca/P ratio (~1.7), spherulitic arrangements of platelets, a rounded crystallite shape, and a crystallite size of around 5 nm. Moreover, there is no preferential growth direction or oriented crystallite assembly. This structure is similar to the structure found in aortic calcifications at atomic/nanometric and microscopic levels, apart from the presence of organic matrix in aortic

calcifications. For example, studies of calcifications in the iliac arteries of patients with uremia showed the presence of spherullites and a microstructure of planar formations composed of rounded nanocrystals with a size of 2 to 10 nm (29). The crystalline phase in the referenced study was mostly apatite, together with whitlockite, which was only detected by using a very intense x-ray source such as synchrotron radiation. This crystallite structure is also found in spontaneous calcium phosphate precipitations, and it can therefore be produced without the intervention of foreign substances. The structure of the deposits gives some clues about the precipitation conditions. The small crystallite size suggests intense nucleation and short crystal growth periods; the planar shape is consistent with crystallization from amorphous calcium phosphate precursors; and the high Ca/P ratio indicates a complete amorphous calcium phosphate to hydroxyapatite conversion. Live cell deposits show similar macroscopic and microscopic structures. However, at atomic and nanometric levels, there are significant differences: amorphous calcium phosphate is present in large amounts, the Ca/P ratio is low (~ 1.4), and crystalline domains are strikingly fiber-shaped. Elongated crystals are found in synthetic crystals of various sizes and are very common in physiological biomineralizations. However, the direction of elongation is usually the [001], while here the fibers are elongated along the perpendicular direction (apparently the [110] direction). Moreover, regarding enamel, rod crystals are formed by a templated assembly of spherical crystals induced by the amel protein (44), whereas here the elongated shape appears at the very first instance of nucleation. In fact, the presence of bent grooves suggests the intervention of flexible organic macromolecules that self-assemble with Polner's clusters, thereby forcing the alignment of these clusters and the formation of fibrillar nuclei. Furthermore, as shown in Fig. 1, the total amount of deposited mineral is substantially less in live cells than in lysed cells. On the other hand, the presence of other hydrated calcium phosphate species in live cells, in addition to apatite, contradicts previous *in vitro* works (11) but agrees with some *in vivo* studies (13, 29, 36). These hydrated species are deficient in Ca^{2+} but rich in oxygen, thereby resulting in a Ca/Pi index of about 1.4, and they can be considered to be hydroxyapatite precursors (7, 10). This indicates that the crystallization process in live cells is at an early stage, most likely as a consequence of a reaction by cells to avoid calcification. Indeed, VSMC cells can reduce the free calcium content in the medium by several mechanisms. For instance, they can do so through the matrix-Gla protein (MGP), which acts as a local calcification inhibitor by calcium sequestration (15). In

addition, the expressions of transient receptor potential calcium channels (TRPCs) and of vanilloid receptor channels (TRPVs) can assist in this process. In conclusion, live cells have a strong influence on CaP crystallization in three ways: 1) by reducing the precipitation rate, 2) by restraining the amorphous calcium phosphate to hydroxyapatite conversion, and 3) by templating the crystal nucleation process. Promoters, inhibitors, and templates of crystallization are omnipresent in physiological and pathological biomineralization processes (7, 8, 22, 25, 34). In fact, normal human serum is supersaturated with respect to hydroxyapatite, OCP, and carbonate apatite, but normal vascular cells have the capacity to inhibit CaP precipitation (8). Actually, the role of inhibitors in preventing mineralization in noncalcifying tissues is generally assumed (22), whereas the lack of inhibitors is considered an important risk factor for pathological calcifications (34). There may be several types of substances that induce the changes to hydroxyapatite crystallization observed in live cell deposits. Effects 1) and 2) can be produced by calcium ligands such as citrate or pyrophosphate or by macromolecules containing carboxylate, sulfate, or phosphate residues. However, effect 3) requires a high templating capacity that is usually exerted by proteins such as collagen, elastin, osteopontin, etc.

In summary, our data point to an intermediate scheme in the calcification process, i.e., between the loss-of-inhibitors hypothesis and the view that calcification is an active, orchestrated process. While calcium phosphate deposition seems to be a passive phenomenon starting with the local loss of calcification inhibitors, CPD actually induces the expression of key osteogenes that modulate the biomineralization of the ECM in a specific crystalline structure. Several important questions, however, remain to be answered. For example, we need to decipher the mechanisms that lead to the initial deposition of calcium phosphates and the loss of local inhibitors that seem to precede calcification. In addition, further research is necessary to make a detailed comparison of the crystallite structure of *in vitro* and *in vivo* aortic VSMC calcification, at a resolution that is at least as high as the one used in this study. Similarly, it is also necessary to understand the specific roles that osteogenes play in the calcification process, because the difference between dead or metabolically active (live) cells is *only* related to the ultrastructure of the nascent crystals. Cells prevent calcification through the production of potent inhibitors (e.g., Fig. 1), while at the same time they can express specific osteogenes as a response to CPD. Only osteogene-specific deletion will help to understand this apparent dichotomy, but at present active prevention of calcification

463 with inhibitors seems to play an initial and mandatory, key role in the process. For example, gene deletion
464 of the local inhibitor MGP induces calcification in arteries under homeostatic Pi conditions (15), and VC is
465 also observed under normal Pi concentrations if other uremic toxins are present (17). Therefore, even
466 under normal Ca and Pi concentrations, CPD seems to be an inevitable phenomenon over time, which
467 arteries attempt to prevent by using mechanisms that need to be deciphered. Whether osteogene
468 expression plays an active role in the pathogenesis of vascular calcification or, conversely, it is only a
469 non-pathological response to CPD, is a point of debate that needs to be definitively clarified.

470

471

ACKNOWLEDGMENTS

None.

GRANTS

This work was supported by a grant from the Spanish Ministry of Science and Innovation (BFU2009-12763/BFI to VS), research grant MAT2007-61621 from the Spanish CICYT Project Consolider-Ingenio in Molecular Nanoscience CSD2007-00010 from the Spanish Ministry of Science, and a predoctoral fellowship from the Government of Aragón, Spain (B086/2007 to RVB).

DISCLOSURES

None.

BIBLIOGRAPHY

1. **Becker A, Epple M, Müller KM, Schmitz I** A comparative study of clinically well-characterized human atherosclerotic plaques with histological, chemical, and ultrastructural methods *J Inorg Biochem* 98:2032–2038, 2004.

2. **Chen NX, O'Neill KD, Duan D, Moe SM.** Phosphorus and uremic serum up-regulate osteopontin expression in vascular smooth muscle cells. *Kidney Int* 62:1724-1731, 2002.

3. **De Maeyer EA, Verbeeck RM, Vercruysse CW.** Conversion of octacalcium phosphate in calcium phosphate cements. *J Biomed Mater Res* 52: 95-106, 2000.

4. **Demer LL, Tintut Y**. Vascular calcification: pathobiology of a multifaceted disease. *Circulation* 117: 2938–2948, 2008.

5. **Dorozhkin SV** Calcium orthophosphates *J Mater Sci* 42: 1061-1095, 2007.

6. **Filgueiras MRT, Mkhonto D, de Leeuw NH** Computer simulations of the adsorption of citric acid at hydroxyapatite surfaces *J Crystal Growth* 294:60–68, 2006.

7. **Gajjeraman S, Narayanan K, Hao J, Qin C, George A**. Matrix macromolecules in hard tissues control the nucleation and hierarchical assembly of hydroxyapatite. *J Biol Chem* 282: 1193-1204, 2007.

8. **Giachelli CM***,* Vascular Calcification Mechanisms *J Am Soc Nephrol* 15:2959-2964, 2004.

9. **Hruska KA, Mathew S, Lund R, Qiu P, Pratt, R**. Hyperphosphatemia of chronic kidney disease. *Kidney Int* 74: 148–157, 2008.

10. **Johnsson MS, Nancollas GH**. The role of brushite and octocalcium phosphate in apatite formation. *Crit Rev Oral Biol Med* 3: 61-82, 1992.

11. **Jono S, McKee MD, Murry CE, Shioi A, Nishizawa Y, Mori K, Morii H, Giachelli CM.** Phosphate regulation of vascular smooth muscle cell calcification. *Circ Res* 87: E10-17, 2000.

12. **Kumar R, Prakash KH, Cheang P, Khor KA** Temperature Driven Morphological Changes of Chemically Precipitated Hydroxyapatite Nanoparticles *Langmuir* 20:5196-5200, 2004.

13. **LeGeros RZ, Contiguglia SR, Alfrey AC**. Pathological calcifications associated with uremia: two types of calcium phosphate deposits. *Calcif Tissue Res* 13: 173-185, 1973.

14. **Liam C. Palmer, Christina J. Newcomb CJ, Kaltz SR, Spoerke ED, Stupp SI** Biomimetic Systems for Hydroxyapatite Mineralization Inspired By Bone and Enamel *Chem Rev* 108:4754–4783, 2008.

15. **Luo G, Ducy P, McKee MD, Pinero GJ, Loyer E, Behringer RR, Karsenty G.** Spontaneous calcification of arteries and cartilage in mice lacking matrix GLA protein. *Nature* 386: 78-81, 1997.

16. **Monma H, Kamiya T**. Preparation of hydroxyapatite by the hydrolysis of brushite. *Journal of Materials Science* 22: 4247-4250, 1987.

17. **Moe SM, Chen NX**. Mechanisms of vascular calcification in chronic kidney disease. *J Am Soc Nephrol* 19: 213-216, 2008.

18. **Nassif N, Martineau F, Syzgantseva O, Gobeaux F, Willinger M, Coradin T, Cassaignon S, Azaïs T, Giraud-Guille MM** In Vivo Inspired Conditions to Synthesize Biomimetic Hydroxyapatite *Chem Mater* 22: 3653–3663, 2010.

19. **O'Neill WC**. The fallacy of the calcium-phosphorus product. *Kidney Int* 72: 792–796, 2007.

20. **O'Neill WC, Mhairi K. Sigrist MK, McIntyre CW**. Plasma pyrophosphate and vascular calcification in chronic kidney disease. *Nephrol Dial Transplant* 25: 187-191, 2010.

21. **Olsson LF, Sandin K, Odselius R, Kloo L** In Vitro Formation of Nanocrystalline Carbonate Apatite – A Structural and Morphological Analogue of Atherosclerotic Plaques *Eur J Inorg Chem* 2007:4123–4127.

22. **Oner M, Dogan O** Inhibitory effect of polyelectrolytes on crystallization kinetics of hydroxyapatite in *Progress in Crystal Growth and Characterization of Materials* 50:39-51, 2005.

23. **Prakash KH, Ooi CP, Kumar R, Khor KA, Cheang P** Effect of Super Saturation Level on the size and morphology of Hydroxyapatite precipitate *IEEE Conference on Emerging Technologies - Nanoelectronics, pp. 345−349 (IEEE, 2006).*

24. **Rakovan J** Growth and Surface Properties of Apatite *Rev Mineral Geochem* 48;51-86, 2002.

25. **Robertson WG** The solubility concept. *In Biological Mineralization and Demineralization*; Nancollas, G. H., Ed.; Springer-Verlag: Berlin, 1981; Chapter 1.

26. **Rodriguez-Lorenzo LM, Vallet-Regi M** Controlled crystallization of calcium phosphate apatites *Chem Mater* 12:2460-2465, 2000.

27. **Schinke T, McKee MD, Karsenty G**. Extracellular matrix calcification: where is the action? *Nat Genet* 21: 150-151, 1999.

28. **Schinke T, Amling M**. Mineralization of bone: An active or passive process? In: *Handbook of Biomineralization*, edited by Epple M, Baeuerlein E. Weinheim (Germany): Wiley-VCH Verlag GmbH & Co, 2007, p. 3-17.

29. **Schlieper G, Aretz A, Verberckmoes SC, Krügen T, Behets GJ, Ghadimi R, Weirich TE, Rohrmann D, Langer S, Tordoir JH, Amann K, Westenfeld R, Brandenburg VM, D'Haese PC, Mayer J, Ketteler M, McKee MD, Floege J** Ultrastructural analysis of vascular calcifications in uremia. *J Am Soc Nephrol* 21: 689-696, 2010

30. **Schoppet M, Shroff RC, Hofbauer LC, Shanahan CM**. Exploring the biology of vascular calcification in chronic kidney disease: What's circulating? *Kidney Int* 73: 384–390, 2008.

31. **Secklera MM, Danese M, Derenzo S, Valarelli JV, Giulietti M, Rodríguez-Clemente R** Influence of Process Conditions on Hydroxyapatite Crystallinity Obtained by Direct Crystallization *Mat Res* 2: 59-62, 1999.

32. **Shanahan CM.** Inflammation ushers in calcification: A cycle of damage and protection? *Circulation* 116: 2782-2785, 2007.

33. **Shroff RC, McNair R, Skepper JN, Figg N, Schurgers LJ, Deanfield J, Rees L, Shanahan CM.** Chronic mineral dysregulation promotes vascular smooth muscle cell adaptation and extracellular matrix calcification. *J Am Soc Nephrol* 21: 103-112, 2010

34. **Silverman LD, Saadia M, Ishal JS, Tishbi N, Leiderman E, Kuyunov I, Recca B, Reitblat C, and Viswanathan R** Hydroxyapatite Growth Inhibition by Osteopontin Hexapeptide Sequences *Langmuir* 26:9899–9904, 2010.

559 35. **Teshima K, Lee S, Sakurai M, Kameno Y, Yubuta K, Suzuki T, Shishido T, Endo M, Oishi S**
560 Well-Formed One-Dimensional Hydroxyapatite Crystals Grown by an Environmentally Friendly Flux
561 Method *Crystal Growth & Design* 9: 2937–2940, 2009.

562 36. **Verberckmoes SC, Persy V, Behets GJ, Neven E, Hufkens A, Zebger-Gong H, Müller D, Haffner**
563 **D, Querfeld U, Bohic S, De Broe ME, D'Haese PC.** Uremia-related vascular calcification: more than
564 apatite deposition. *Kidney Int*. 71: 298-303, 2007.

565 37. **Villa-Bellosta R, Bogaert YE, Levi M, Sorribas V**. Characterization of phosphate transport in rat
566 vascular smooth muscle cells: implications for vascular calcification. *Arterioscler Thromb Vasc Biol*
567 27: 1030-1036, 2007.

568 38. **Villa-Bellosta R, Sorribas V**. Different effects of arsenate and phosphonoformate on P(i) transport
569 adaptation in opossum kidney cells. *Am J Physiol Cell Physiol* 297: C516-C525, 2009.

570 39. **Villa-Bellosta R, Sorribas V**. Phosphonoformic acid prevents vascular smooth muscle cell
571 calcification by inhibiting calcium-phosphate deposition. *Arterioscler Thromb Vasc Biol* 29: 761-766,
572 2009.

573 40. **Villa-Bellosta R, Sorribas V**. Compensatory regulation of the sodium/phosphate cotransporters
574 NaPi-IIc (SCL34A3) and Pit-2 (SLC20A2) during Pi deprivation and acidosis. *Pflugers Arch* 459: 499-
575 508, 2009.

576 41. **Villa-Bellosta R, Levi M, Sorribas V**. Vascular smooth muscle cell calcification and SLC20 inorganic
577 phosphate transporters: effects of PDGF, TNF-alpha, and Pi. *Pflugers Arch* 458: 1151-1161, 2009.

578 42. **Yang H, Curinga G, Giachelli CM**. Elevated extracellular calcium levels induce smooth muscle cell
579 matrix mineralization in vitro. *Kidney Int* 66: 2293-2299, 2004.

580 43. **Wang L, Nancollas GH** Calcium Orthophosphates: Crystallization and Dissolution *Chem Rev*
581 108:4628–4669, 2008.

582 44. **Wang L, Guan X, Yin H, Moradian-Oldak J, Nancollas GH** Mimicking the Self-Organized
583 Microstructure of Tooth Enamel *J Phys Chem C* 112:5892-5899, 2008.

584

585 **FIGURES**

586 **Figure 1.** Calcification of VSMC *in vitro*. A. Incubation of live (open bars) and fixed (black bars, 3%
587 paraformaldehyde) VSMC with MEM containing 2 mM Pi, for the indicated times. B. Kinetic analysis of the
588 effect of PPi on the calcification of live cells (squares) and fixed cells (triangles), showing fits to sigmoidal,
589 dose-response curves. The subtraction of both curves provides a Gaussian fit (bold line). *Significantly
590 different from the corresponding value at 1 day.

591 **Figure 2**. Proteins involved in vascular calcification. A. Effect of detergents on cells incubated with 2 mM
592 Pi for up to 5 days. Every day a group of cells were either trypsinized or treated with the indicated
593 detergents and saponine, all of them at 0.1 %. Calcification was visualized with alizarin red. B.
594 Quantification of the calcium content in cells treated as indicated during seven days in MEM with 2 mM
595 Pi. C. Alizarin red staining of collagen I, elastin, albumin or poly-L-lysine attached to a plastic support and
596 incubated with 1 or 2 mM for seven days.

597 **Figure 3.** Effect of cell culture composition, pH and Ca x P products. A. Effect of 2 mM Pi on the
598 calcification of fixed VSMC using MEM, DMEM, and DMEM/F:12. B. Effect of pH on 2 mM Pi-induced
599 calcification in lysed VSMC cells using DMEM/F:12, supplemented to contain 1.8 mM $CaCl_2$. C.
600 Calcification using DMEM/F:12 with 2 mM Pi in live (open bars) and fixed (black bars) OK cells for the
601 indicated times. D. Calcification takes place when Ca x Pi products are obtained with 2x2 or 4x1 mM Ca x
602 Pi. Cells were fixed with 3% paraformaldehyde.

603 **Figure 4**. Role of calcium and media components on calcification. A. Calcification of fixed VSMC with
604 increasing concentrations of Ca^{2+} and a constant Pi (1 mM). Cells were fixed with 3% paraformaldehyde.
605 B. Calcification induced with increasing concentrations of Pi, at three fixed concentrations of Ca^{2+}: 1.5,
606 1.8, and 2 mM. C. Effect of MEM components on Pi-induced calcification: aa+vit, amino acids plus
607 vitamins; SC, salt component; Glc, glucose. D. Analysis of the effect of the salt component of MEM
608 culture media on Pi-induced calcification in VSMC.

609 **Figure 5**. Osteogene RNA expression during calcification. A. Expression of Bmp2, Cbfa1, Msx2, and Osx
610 in VSMC incubated with sMEM for 24 hours with 1.8 mM Ca^{2+} plus 1 or 2 mM Pi. B. Expression of the four
611 genes as a function of the number of days of treatment with 2 mM Pi. *Significantly different from the

612 corresponding 1 mM Pi ($p < 0.05$). C. Expression of Cbfa1, Bmp2, and Sm22α in the presence of the
613 indicated combinations of Ca^{2+} and Pi, in mM, for three days. Cbfa1 and Bmp2 are only induced when the
614 combination of Ca^{2+} and Pi leads to CPD, as shown in Fig. 2D. *Significantly different from 2 mM Ca^{2+}+1
615 mM Pi ($p<0.05$).

616 **Figure 6**. Analysis of the crystal composition in mineralized live and lysed cells. A. XRD patterns of lysed
617 and live powdered deposit samples; bars correspond to the hydroxyapatite crystal structure. B and C,
618 SEM images or deposits from lysed (B) and live (C) cell cultures. Cells were lysed with 3%
619 paraformaldehyde.

620 **Figure 7.** Transmission electron microscopy analysis of crystalline domains. A and C, deposits of lysed
621 and live cells; insets show higher magnification revealing granular and fibrillar structures, respectively. B
622 and D, HRTEM images of lysed and live cell deposits, showing the difference between rounded
623 crystalline domains in lysed cells and long fibers in live cells. Cells were lysed with 3% paraformaldehyde.

624 **Figure 8.** Fast Fourier transform of atomic resolution HRTEM images of (A) a polycrystalline area from a
625 lysed cell deposit sample; and (B) a fiber-nanocrystal from a live cell deposit sample. C. HRTEM image of
626 an area of a live cell deposit sample showing parallel bent grooves that can be interpreted as an
627 intermediate stage of fiber-crystal formation process.

628

Figure 1

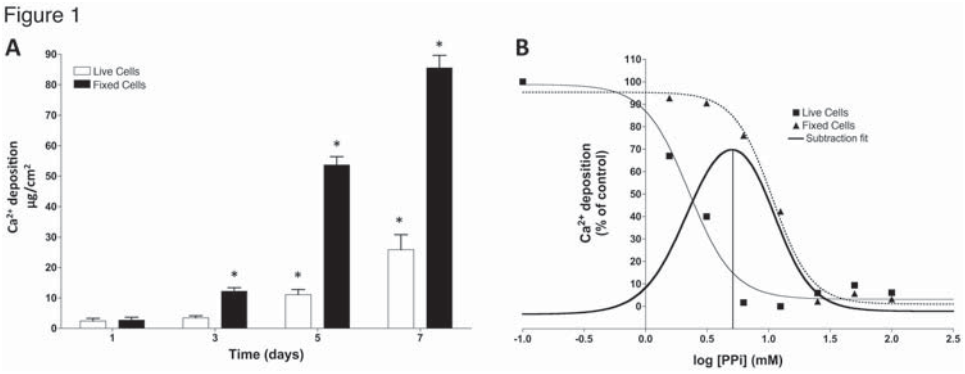
A
Live Cells
Fixed Cells
Ca2+ deposition
µg/cm2
Time (days)
B
Live Cells
Fixed Cells
Subtraction fit
Ca2+ deposition
(% of control)
log [PPi] (mM)

Figure 2

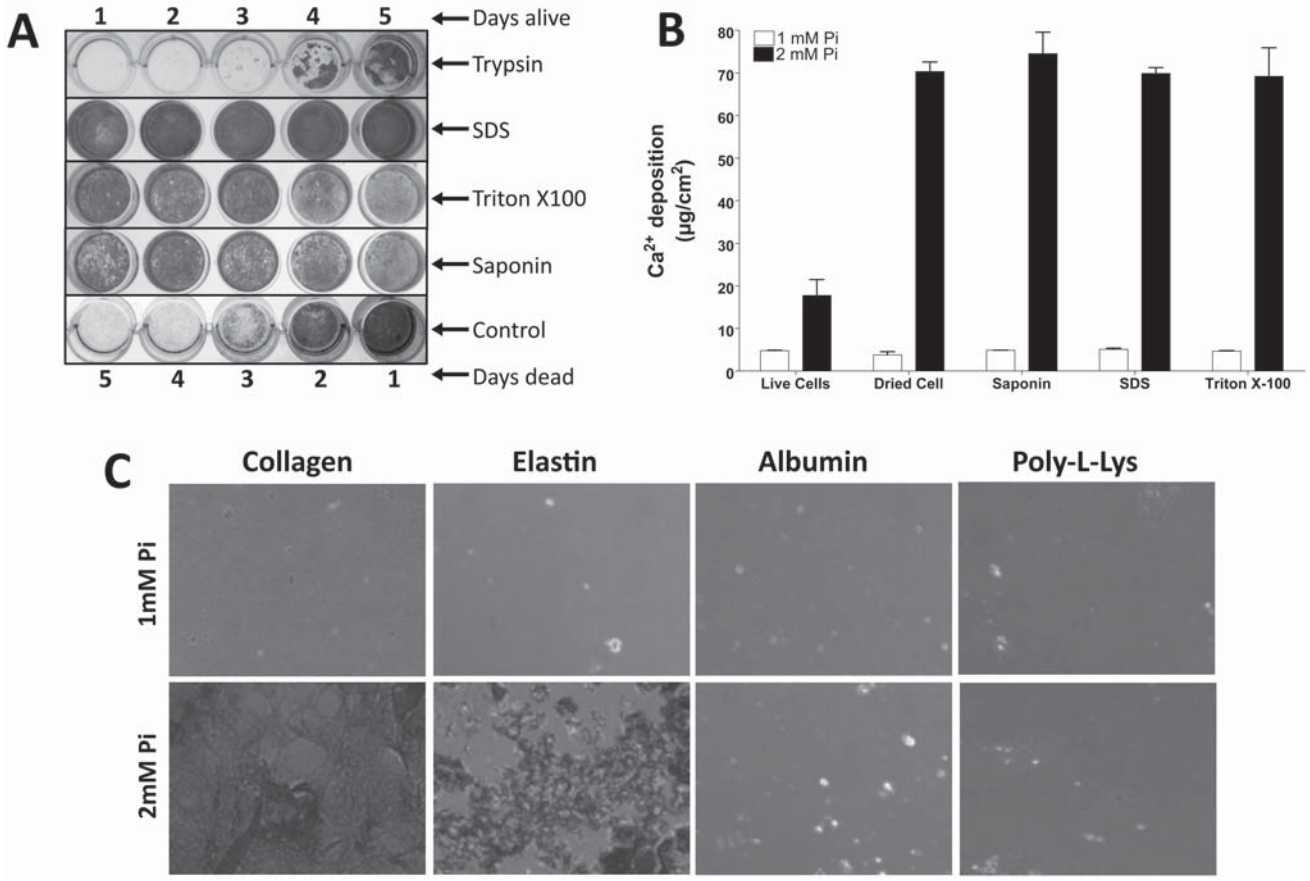
A
1 2 3 4 5
Days alive
Trypsin
SDS
Triton X100
Saponin
Control
5 4 3 2 1
Days dead
B
1 mM Pi
2 mM Pi
Ca2+ deposition (µg/cm2)
0 10 20 30 40 50 60 70 80
Live Cells
Dried Cell
Saponin
SDS
Triton X-100
C
Collagen
Elastin
Albumin
Poly-L-Lys
1mM Pi
2mM Pi

Figure 3

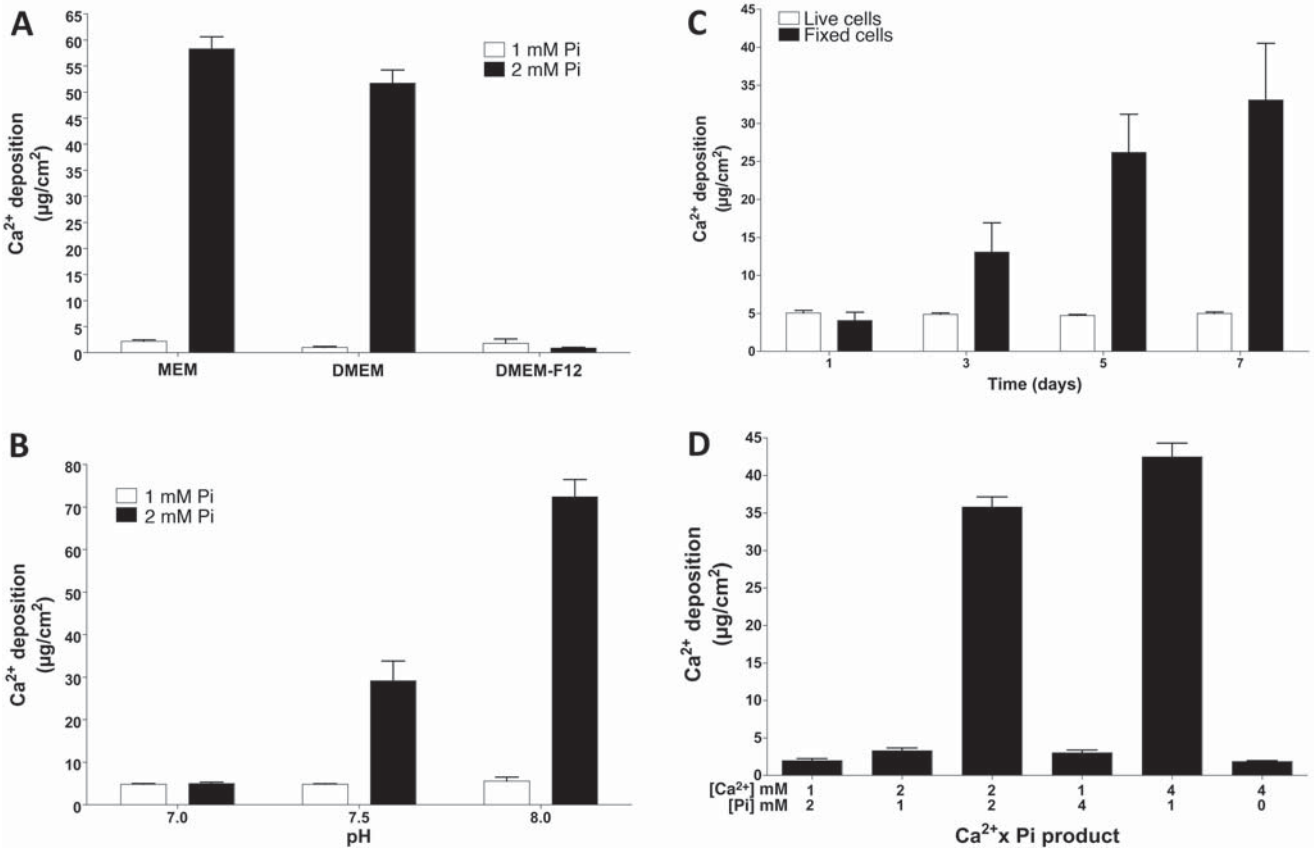
A
1 mM Pi
2 mM Pi
Ca2+ deposition (µg/cm2)
MEM
DMEM
DMEM-F12
B
1 mM Pi
2 mM Pi
Ca2+ deposition (µg/cm2)
7.0
7.5
8.0
pH
C
Live cells
Fixed cells
Ca2+ deposition (µg/cm2)
Time (days)
D
Ca2+ deposition (µg/cm2)
[Ca2+] mM 1 2 2 1 4 4
[Pi] mM 2 1 2 4 1 0
Ca2+x Pi product

Figure 4

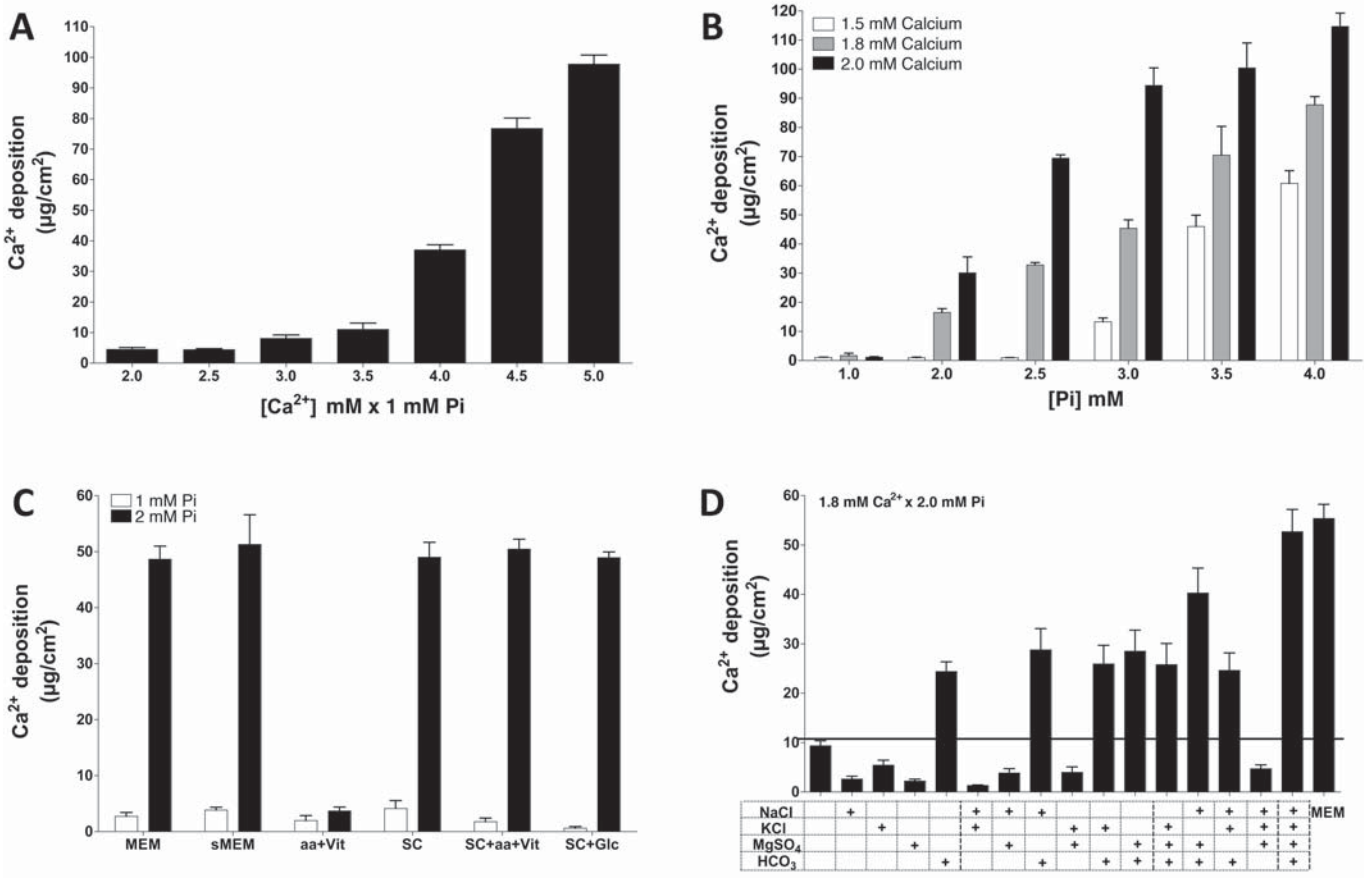
A
Ca2+ deposition (µg/cm2)
[Ca2+] mM x 1 mM Pi
B
1.5 mM Calcium
1.8 mM Calcium
2.0 mM Calcium
Ca2+ deposition (µg/cm2)
[Pi] mM
C
1 mM Pi
2 mM Pi
Ca2+ deposition (µg/cm2)
MEM
sMEM
aa+Vit
SC
SC+aa+Vit
SC+Glc
D
1.8 mM Ca2+ x 2.0 mM Pi
Ca2+ deposition (µg/cm2)
NaCl
KCl
MgSO4
HCO3
MEM

Figure 5

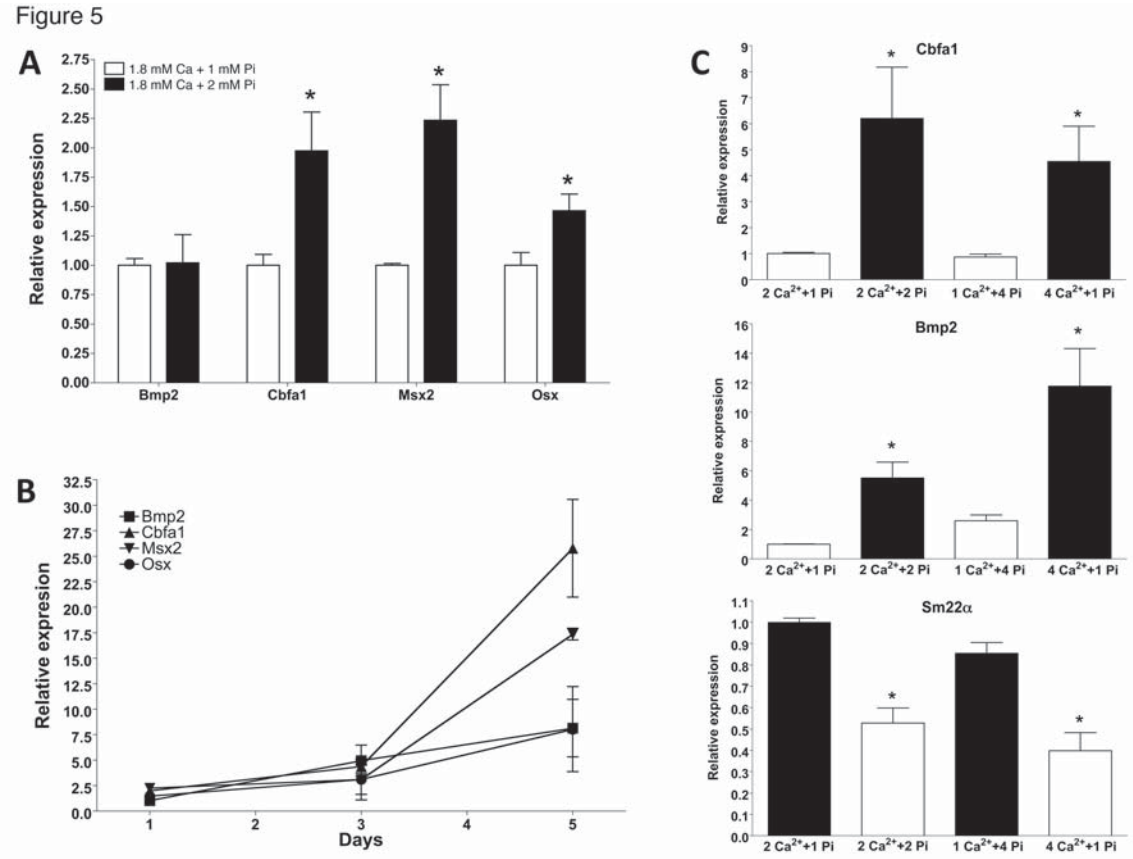
A
1.8 mM Ca + 1 mM Pi
1.8 mM Ca + 2 mM Pi
Relative expression
Bmp2
Cbfa1
Msx2
Osx
B
Bmp2
Cbfa1
Msx2
Osx
Relative expression
Days
C
Cbfa1
Bmp2
Sm22α
Relative expression
2 Ca2+1 Pi
2 Ca2+2 Pi
1 Ca2+4 Pi
4 Ca2+1 Pi

Figure 6

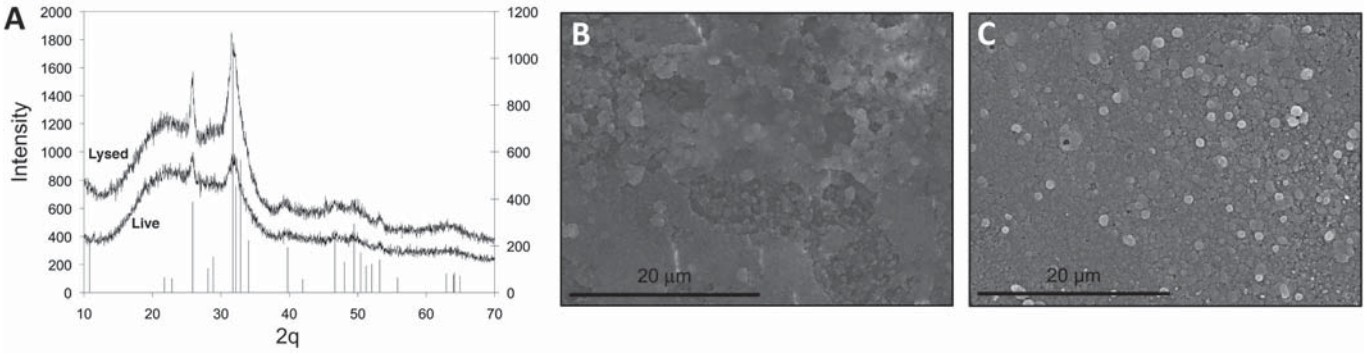

Figure 7

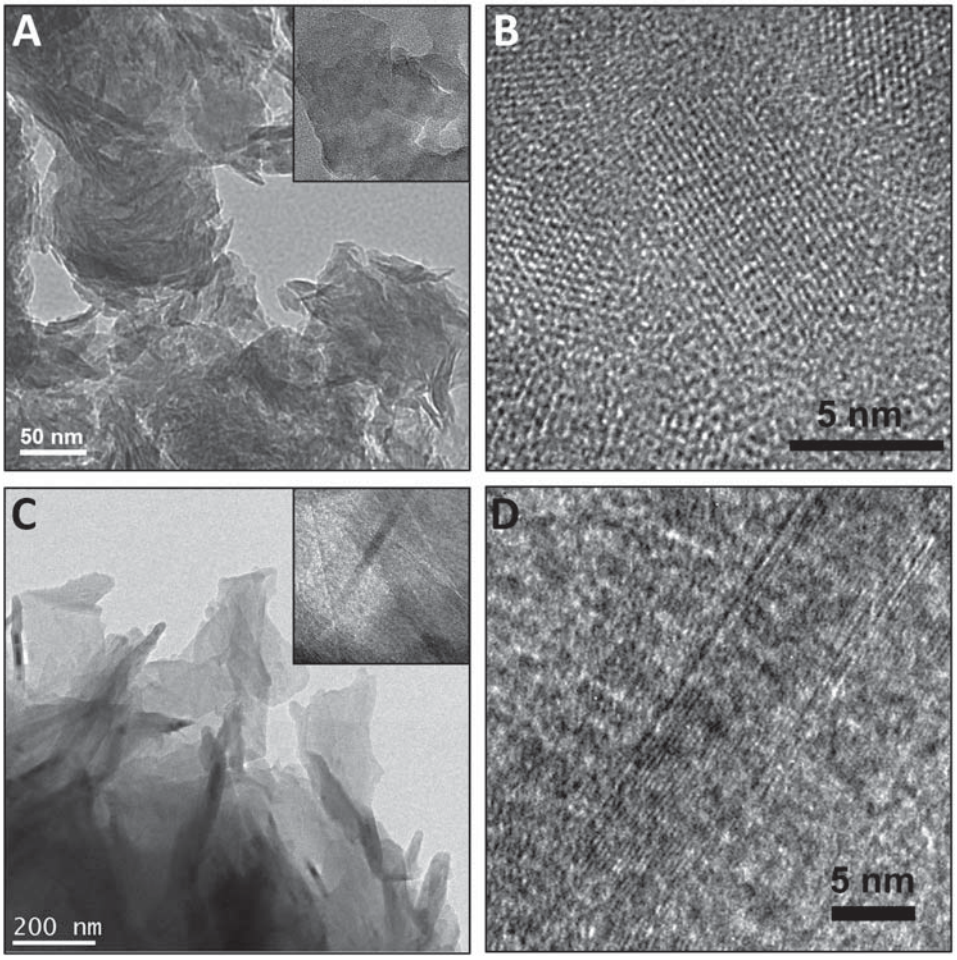

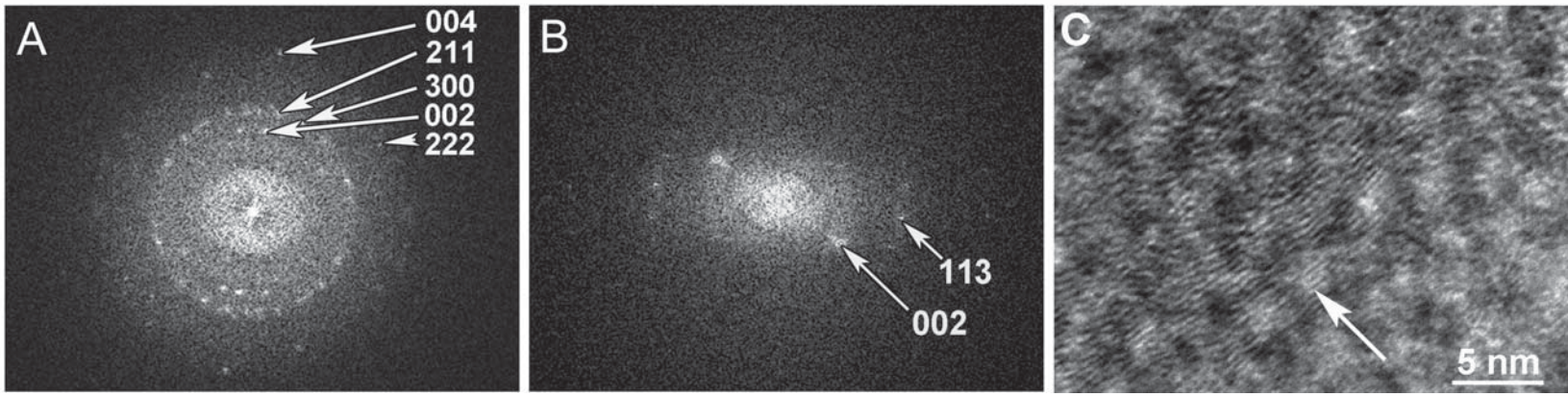
A
004
211
300
002
222
B
113
002
C
5 nm